CrossMark

ORIGINAL PAPER

Long-term monitoring of reinforced earth structures using distributed fiber optic sensing

Florian Moser[1] · Werner Lienhart[1] · Helmut Woschitz[1] · Hartmut Schuller[2]

Abstract Reinforced earth structures are commonly used to construct earth structures with high inclination angles. The stability and safety of such constructions is highly dependent on the strain distribution of the geogrids inside the earth structure. In this article, we report about the development and implementation of a structural monitoring system to measure the strain distribution of geogrids with high accuracy and high spatial resolution. The system was developed for the Semmering Base Tunnel project in Austria but can also be applied to other reinforced earth structures. The Semmering Base Tunnel is one of the core infrastructure projects in central Europe. Prior to the start of the actual tunnel excavation, comprehensive preparatory works in the alpine landscape were necessary. One of these works included the relocation of a river stream at the disposal site Longsgraben. To establish this relocation, a reinforced earth structure with a total length of more than 1.3 km and heights up to 25 m was constructed. To evaluate the stability of this structure, a monitoring system was developed. This monitoring system is thereby based on external geodetic and internal distributed fiber optic measurements. For the latter, about 2 km of Brillouin sensing cables in several sensor sections were installed in the project area. In this paper, we report about the laboratory experiments to determine strain and temperature coefficients for the conversion of the measured Brillouin frequency shifts into strain or temperature values. Furthermore, the long-term behavior of the monitoring structure is analyzed for the period of 1 year after installation.

Keywords Brillouin sensing · BOFDA · Field application · Calibration · Long-term monitoring

1 Introduction

The Semmering Base Tunnel, which is currently under construction, is one of the core infrastructure projects of Austria. Moreover, it is part of the European TEN-T Core Network Corridor that connects the Baltic and the Adriatic Sea. The Semmering Base Tunnel with a total length of 27.3 km will realize a high-speed rail connection according to the latest requirements for international rail traffic [2] in 2025. Prior to tunnel excavation, several preparatory works were necessary, including a disposal site for 4.25 million m^3 of excavated material. This disposal site is located in the so-called "Longsgraben", an uninhabited narrow valley close to "Fröschnitzgraben", one of the main access points for tunnel construction. Before the tunnel material fills up the narrow valley, the flowing stream had to be relocated from the valley floor to an up to 50 m higher position. For this purpose, reinforced earth structures were built over a length of more than 1.3 km and heights of up to 25 m on the steep slope of the valley.

Because material from 12 tunnel construction access points will be deposited in this one disposal site, any malfunction of this construction will result in a delay of the whole tunneling project. Thus, an appropriate monitoring program was needed.

In this paper, we present the developed monitoring solution to assess the operating grade of the used

✉ Werner Lienhart
  werner.lienhart@tugraz.at

1 Institute of Engineering Geodesy and Measurement Systems, Graz University of Technology, Steyrergasse 30, 8010 Graz, Austria

2 INSITU Geotechnik ZT GmbH, Gartengasse 19, 8010 Graz, Austria

reinforcement. We focus on the calibration results of the fiber optic-based monitoring system and the strain results of more than one year of field measurements.

2 Reinforced earth structures at the disposal site

The excavation material from tunneling will fill up the valley at the disposal site Longsgraben up to more than 50 m. After filling, the new terrain will be afforested and the in advance relocated stream will mark the new valley bottom, see Fig. 1. To realize the relocation, reinforced earth structures are used over a length of about 1.3 km at the steep valley side. The reinforced earth structures feature thereby a slope angle of 60°. A special challenge is the final section of the relocation construction, where the stream is guided back to its original position. In this section, the new stream bed has a slope angle of more than 50 % (Fig. 2). A maintenance road is located at the crown
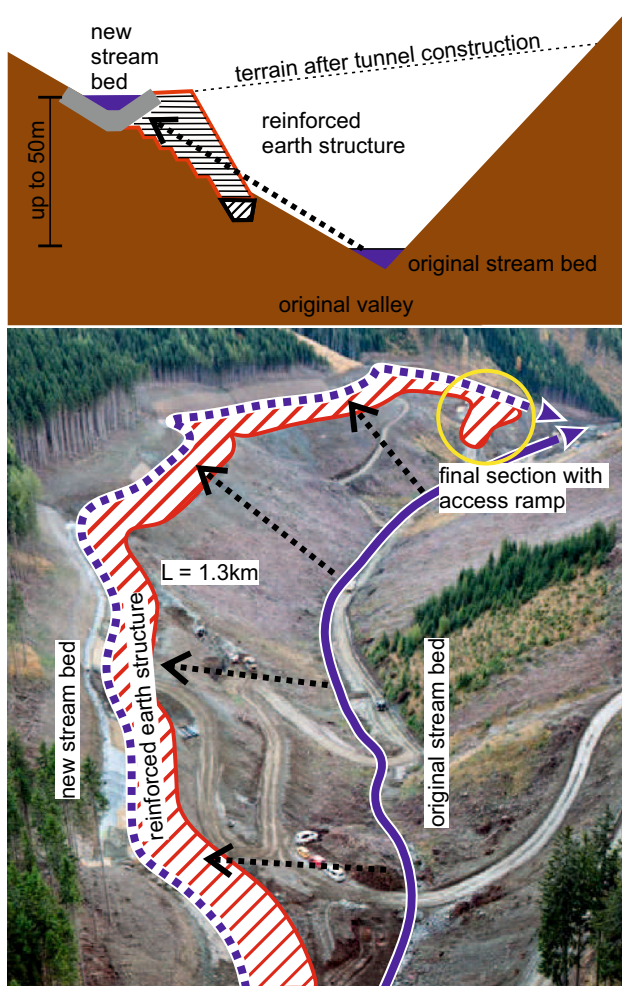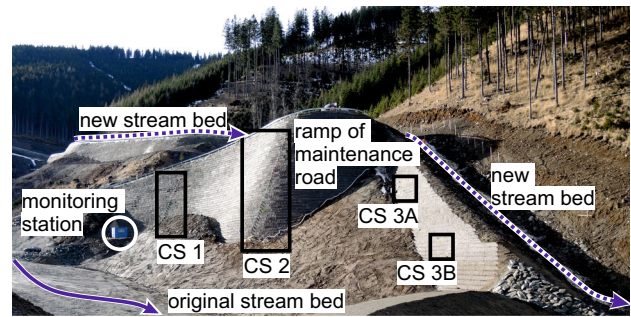

Fig. 2 Monitoring cross sections (CS) at the final section of the stream relocation

of the reinforced earth structure. This road is reachable via a 25-m-high reinforced earth ramp at the final section of the relocation construction (Fig. 2). The earth structures for the relocation and access ramp use geogrids from Huesker Synthetic as reinforcement. The geogrids were dimensioned with the maximum value of tensile strength and strain behavior taken from both, conventional analysis and finite element simulations [8].

A specially designed monitoring system was installed to determine the structural behavior during the installation and after completion of the construction works. The monitoring program included weekly conventional geodetic measurements in various cross sections of the stream relocation. In the critical final section of the relocation construction a fiber optic strain measurement system was additionally installed to monitor the operating grade of the geogrids.

Further details on design and construction of the reinforced earth structures and on the geotechnical monitoring can be found in [6] or in more detail in [9].

3 Measurement system

Since the aim of the project was to determine the operating grade of the used geogrids, a measurement system which is integrable into the earth structure and mountable to the geogrids had to be used. As the exact type of geogrids was unknown until the beginning of the construction works, none of the existing monitoring systems could be used. Based on these requirements a monitoring solution using fiber optic measurements was developed by the Institute of Engineering Geodesy and Measurement Systems (IGMS) of Graz University of Technology. The uncertainty of the fiber optic strain measurement should be less than 0.1 %. A detailed description of the used components can be found in [6].

The monitoring program focuses on four cross sections (CS). Two cross sections (CS 3A and CS 3B) are located in

Fig. 1 Reinforced earth structure to relocate the natural stream bed at the Longsgraben valley

the final section of the relocation construction, see Fig. 2. The other two cross sections (CS 1 and CS 2) are located in the reinforced earth ramp of the maintenance road. In the cross sections, up to five levels are equipped with sensing cables. Each level is thereby subdivided by adapters into segments [2–7 level segments (ls) per level]. At the end of the construction works we have installed almost 100 measurement segments.

Due to the large size of the monitoring object and the high number of measurement segments it was decided to use a distributed Brillouin backscattering system. Brillouin scattering occurs when light traveling in a single-mode optical fiber is reflected by the refractive index modulations produced by acoustic waves (e.g., [3] or [7]). In our application, the scattered light is recorded and the frequency is analyzed with a spatial resolution of 0.5 m by a Brillouin optical frequency-domain analysis (BOFDA) interrogation unit (Fibris Terre fTB2505). Through determination of frequency changes between two measurement epochs it is in our setup possible to calculate strain and temperature variations.

Figure 3 shows exemplarily the Brillouin frequency spectrum for a 60-m-long fiber. Clearly visible is the center frequency of about 10.55 GHz of the unstrained fiber. In this example, strain was applied to different sections (25, 36 and 42 m) of the fiber, which results in significant shifts of the Brillouin frequency.

Since the BOFDA measurement principle requires a closed loop, each measurement level of the reinforced earth structure consists of a forward and a return path, see Fig. 4 left. The forward path was pre-strained during installation and is consequently sensitive to both temperature and strain. The stress-free installed return path is only sensitive to temperature changes. By combining both sides a temperature compensation is realized. However, the

Fig. 3 Brillouin frequency spectrum along an optical sensing fiber

measurements cannot be performed if the fiber loop is interrupted at any location. Therefore, installations in harsh environments require a robust sensing cable to be embedded into the earth structure and a well-trained installation crew. In our application, a total of 2 km of the sensing cable BRU-Strain V4 from Brugg Cables were installed. Using specially designed adapters an appropriate connection to the geogrids could be realized. Extensive laboratory investigations confirmed a reliable strain transfer from the geogrid to the fiber core [6].

4 System calibration

The detected Brillouin frequency linearly depends on longitudinal strain [3] and temperature [4]. Therefore, the change in the detected Brillouin frequency Δv_B between two measurements is a function of strain $\Delta \epsilon$ and temperature ΔT variations:

$$\Delta v_B = \left. \frac{\partial v_B}{\partial \epsilon} \right|_{T=const.} \cdot \Delta \epsilon + \left. \frac{\partial v_B}{\partial T} \right|_{\epsilon=const.} \cdot \Delta T \qquad (1)$$

We introduce the linear strain and temperature coefficients k_ϵ and k_T for the partial derivations

$$k_\epsilon = \left. \frac{\partial v_B}{\partial \epsilon} \right|_{T=const.} \qquad (2)$$

$$k_T = \left. \frac{\partial v_B}{\partial T} \right|_{\epsilon=const.} \qquad (3)$$

Accurate values for the strain k_ϵ and temperature k_T sensitivities are essential for the accurate determination of longitudinal strain and temperature.

4.1 Strain calibration

The sensor testing process was performed as a sample testing procedure. Since the whole 2 km sensor cable came from the same production series, the calibration value of a section of the cable was considered valid for the whole sensing cable. The testing process was carried out under laboratory conditions in June 2013 prior to the field installation. The sensor cable was installed between two specially designed adapters in the test facility (Fig. 5) with a distance of 1 m between the adapters. The adapter design ensures that the applied strain is axial to the sensor. The strain of the sensor cable was increased in five steps from 0 to 3 %. The reference strain was measured by displacement transducers with a precision of about 10 μm. Since the finite element simulations of the reinforced earth structures showed a high extension of the geogrids, the testing process was performed up to a strain of about 3 %. Figure 6 shows the result of the calibration process with two runs,
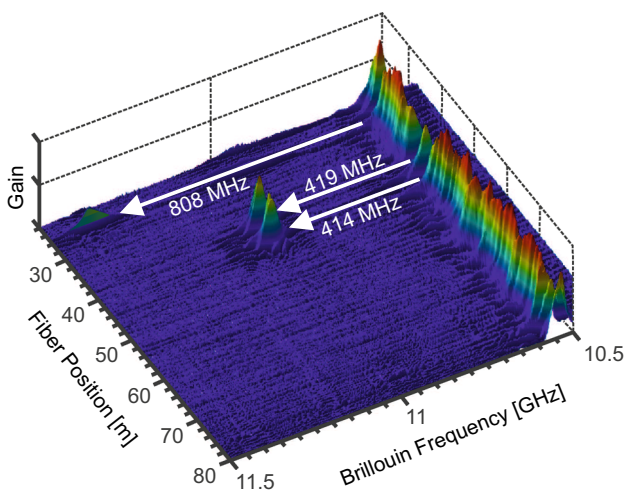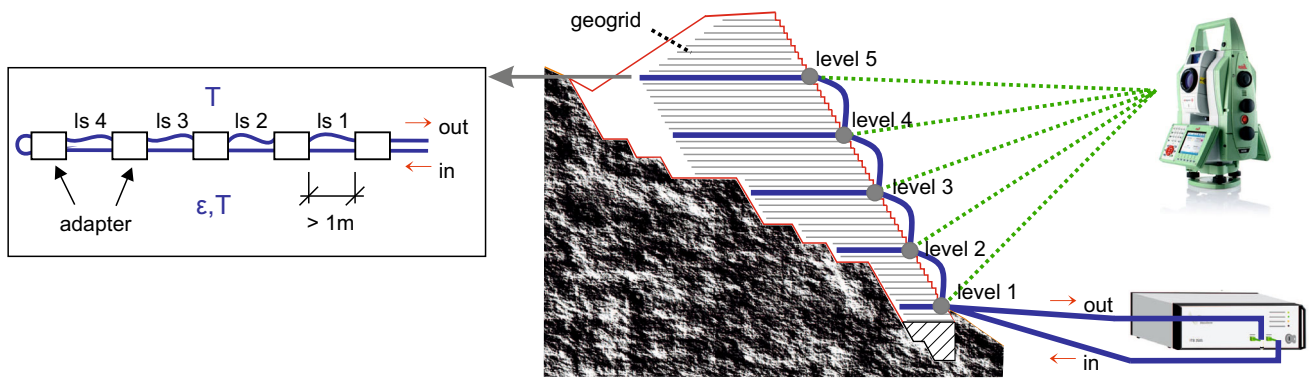
Fig. 4 Monitoring levels in CS 2 with installed fiber optic sensing cable (*right*); level segments (ls) in level 5 (*left*)
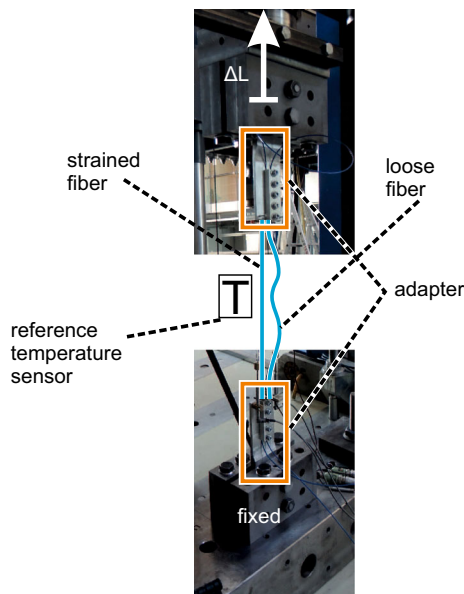

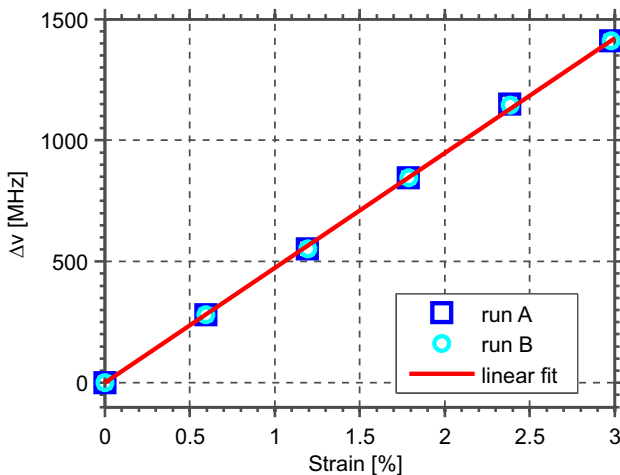**Fig. 5** Strain coefficient determination: sensor testing facility

Fig. 6 Strain coefficient determination: calibration results

which took about 3 h. The results of both runs coincide well, with a maximum deviation of 15 MHz. Using all data, a linear strain dependence of 479 MHz/% was determined by these measurements with a precision of 5 MHz/%. This value is in agreement with the approximate 500 MHz/% stated by the manufacturer [1]. Using the manufacturer coefficient, however, would result in an error of 4 percent of the actual value.

4.2 Temperature calibration

According to [5] the temperature dependency of the Brillouin frequency shift k_T in jacketed single-mode silica fibers consists of the temperature dependency of the Brillouin frequency shift of the bare fiber k_T^* and the frequency shift induced by the thermal strain of the jacketed fiber

$$k_T = \left(k_T^* + k_\epsilon \cdot \frac{\partial \epsilon}{\partial T} \right) \tag{4}$$

The thermal strain in a strain-free fiber is thereby caused by the difference in the thermal expansion coefficients of the bare fiber and the coating material [5]. Temperature changes ΔT can be calculated from the measured frequency shifts of the strain-free fiber if the combined effect k_T is known

$$\Delta T = \frac{\Delta v_B}{k_T} \tag{5}$$

The temperature changes are needed for the subsequent compensation of the measured strain values. To determine k_T, a sensor sample of 10 m length was carefully installed strain free in a climate chamber. In this chamber the temperature was changed in seven steps from 0 to +60 °C, which was the expected range in our application. The reference temperature was measured with two calibrated PT100 temperature sensors. Figure 7 shows the climate chamber and Fig. 8 the results of seven measured temperature cycles. The calculated temperature coefficient of
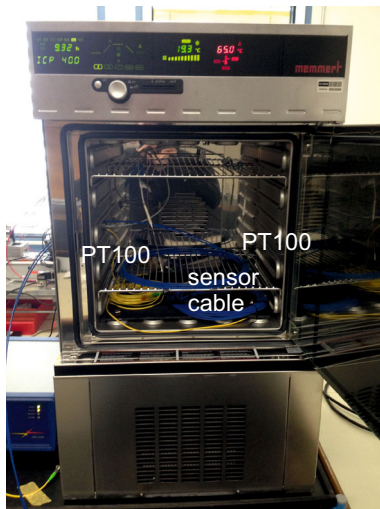
Fig. 7 Temperature coefficient determination: climate chamber with sensor cable and reference temperature sensors (PT100)
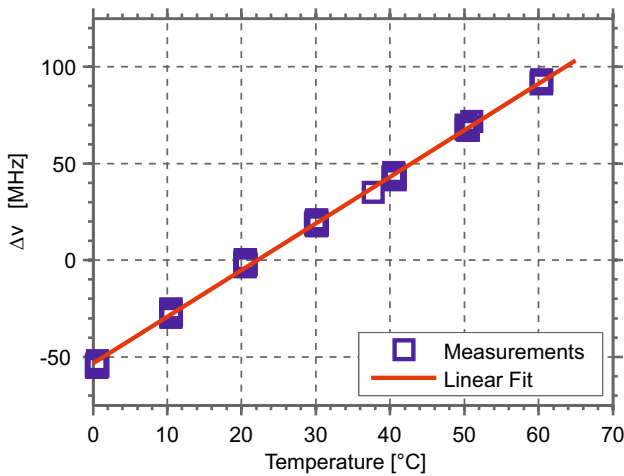

Fig. 8 Temperature coefficient determination: measurement results

the jacketed fiber k_T is 2.41 MHz/K with a precision of 0.01 MHz/K. This value is approximately twice as high as the typical value of the bare fiber ($k_T^* \sim$ 1.2 MHz/K, see e.g., [5]).

5 Field measurements

At the disposal site all measurement segments (ls) in the different levels inside the cross sections (CS) can be measured simultaneously from a central monitoring station. The Brillouin frequencies of the entire 2 km of sensing cable are scanned by a single measurement. The software developed at our institute automatically allocates the measured frequencies to the level segments of the cross sections and calculates the temperature compensated

frequency changes. Finally, the determined calibration functions are used to convert this frequency changes into strain values.

5.1 Spatial allocation

As expected we observed a discrepancy of the spatial allocation of the level segments in measurements of different epochs. Figure 9 shows the detected frequencies of the segments of level 2 of cross section CS 2 for the measurements in February and June 2014. It can be seen that the two signals are shifted by ΔL of about 0.5 m. Such an effect could be caused by various factors. Since the determination of the position along the fiber uses the propagation velocity and the runtime of the signal, it is dependent on the used refractive index n of the sensor fiber. The refractive index, however, is varying with temperature. As a consequence temperature changes between two measurement epochs cause a runtime change. Another possible factor is a length change in prior level sections caused by a deformation of the reinforced earth structure. A further factor can be a physical length change of the coating material with temperature in the fiber sections prior to the strained segments.

In our application, different sections of the sensing cable experience different temperature changes. Connecting cable sections on the surface of the structure are exposed to direct solar irradiation and consequently large temperature differences (ΔT approx. 30 K) over the year. Cable sections inside the reinforced earth structure experience low temperature differences (ΔT approx. 0–10 K) over the year. A correction with a single adjusted refractive index or a correction with a single value for the expansion of the coating material is, therefore, not possible.
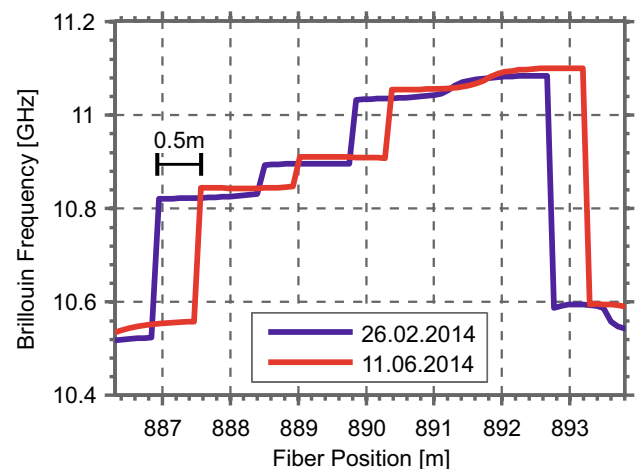

Fig. 9 Spatial allocation discrepancy in the strained section of the 2nd level in CS 2 between the measurements in February and June 2014

For these reasons we corrected for our application the fiber position in post-processing for each level between two measurement epochs by cross correlating the corresponding signals of the level.

5.2 Strain evolution in cross section CS 2

Figure 10a–c shows some temperature and spatially corrected strain results of cross section CS 2 and the strain distribution (Fig. 10d) inside the earth body for a period of about 1 year. In this cross section five geogrid levels were equipped with the fiber optic sensing cable. Displayed is the strain evolution of the first three levels and their position inside the reinforced earth body. The measurements were carried out once a week during the construction phase (until end of November 2013) and sporadically afterwards. Obviously, construction works in the upper levels result in an increase of the geogrid strain in the lower levels of the

reinforced earth structure. During the construction phase the strain increases thereby strongly in all segments. After the completion of the reinforced earth body the strain still continues to increase, but at a much lower rate.

Due to this continuing increase of the strain values and to gather experiences about the performance of the system over several years, the monitoring program will be continued until the disposal site is completely filled with the tunnel excavation material.

Figure 10d shows the accumulated strain inside the reinforced earth structure for the different segments in November 2014. The obtained results show an inhomogeneous strain distribution inside the reinforced earth structure. The highest observed strain can be seen in level 2 of cross section CS 2 with about 1.2 %. Nevertheless, this is much lower than the strain predicted by the finite element analysis, which shows the importance of field measurements for model validation. A comparison between the
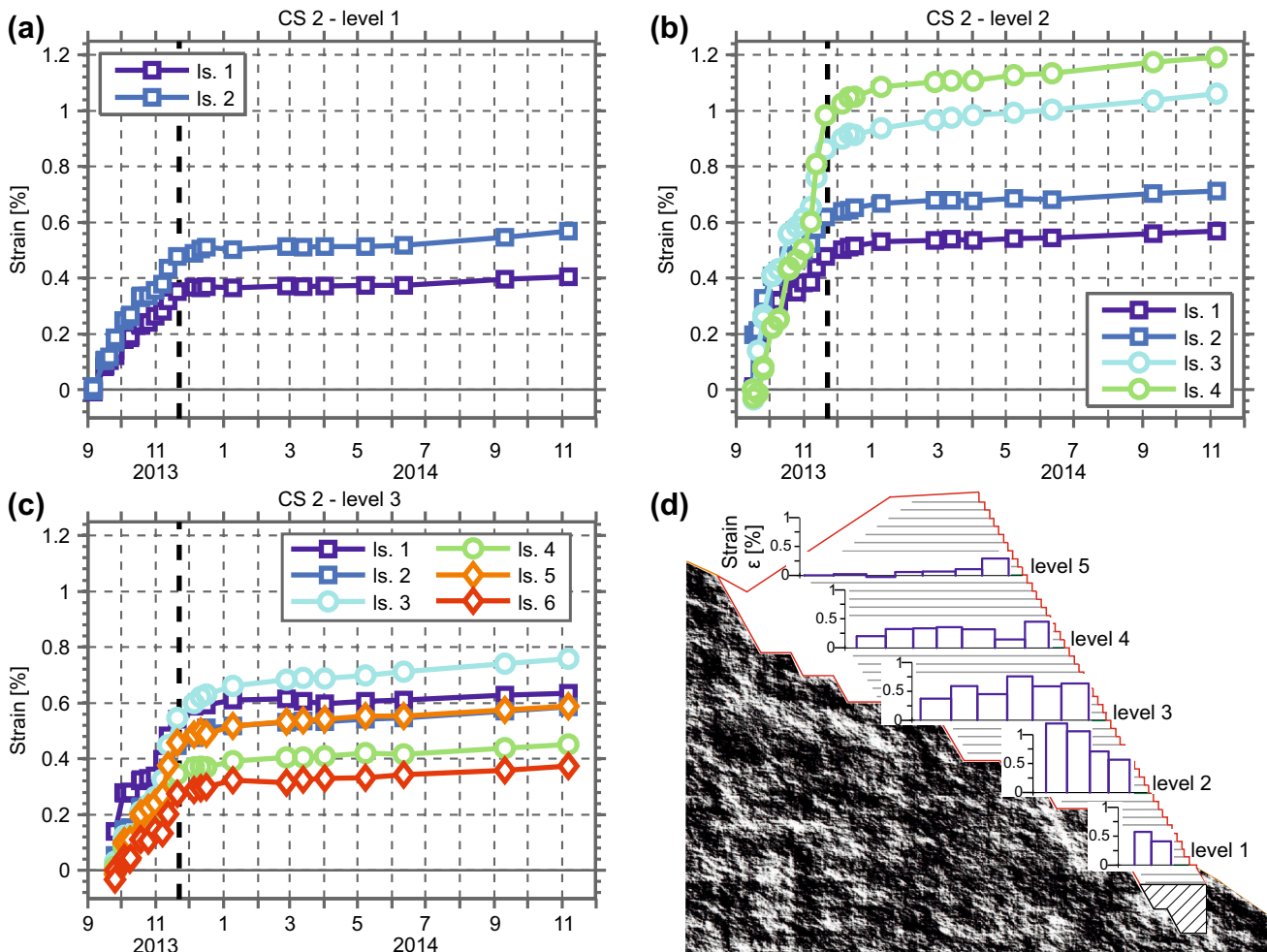

Fig. 10 Strain development of the segments (ls) in the levels 1–3 in cross section CS 2; the *vertical bold dashed line* marks the end of the construction works; the sub-figure in the *bottom right* (d) shows the accumulated strain distribution inside the reinforced earth structure in November 2014

forces predicted by the finite element analysis and the measured fiber optic values can be found in [6] or in more detail in [8].

6 Conclusion

In this paper, we presented a robust monitoring system to measure the inhomogeneous strain distribution inside reinforced earth structures. The developed solution is, especially because of the modular adapters, flexible and can be used with many types of geogrids. It also survived the harsh installation process and is 1 year after installation, with strains up to 1 % and higher, still fully operational.

We also demonstrated the importance of calibration for reliable and accurate distributed fiber optic strain and temperature measurements. Both coefficients for temperature and strain sensitivity have been determined with high precisions ($\sigma_{k_T} = 0.01$ MHz/K and $\sigma_{k_\epsilon} = 5$ MHz/%). Finally it has to be noted that the correct spatial allocation is crucial in long-term monitoring applications.

References

1. Brugg Cables AG (2012) BRUSENS STRAIN V4. VERS. 2012/06/19 REV. 01: Data Sheet
2. Gobiet G (2013) The new Semmering base tunnel—project overview. Geomech Tunnel 6(6):680–687. doi:10.1002/geot.201310022
3. Horiguchi T, Kurashima T, Tateda M (1989) Tensile strain dependence of Brillouin frequency shift in silica optical fibers. IEEE Photon Technol Lett 1(5):107–108
4. Kurashima T, Horiguchi T, Tateda M (1990) Thermal effects of Brillouin gain spectra in single-mode fibers. IEEE Photon Technol Lett 2(10):718–720
5. Kurashima T, Horiguchi T, Tateda M (1990) Thermal effects on the Brillouin frequency shift in jacketed optical silica fibers. Appl Opt 29(15):2219–2222
6. Lienhart W, Moser F, Schuller H, Schachinger T (2014) Reinforced earth structures at Semmering base tunnel—construction and monitoring using fiber optic strain measurements. In: 10th International Conference on Geosynthetics (10ICG)
7. Nöther N (2010) Distributed fiber sensors in river embankments: advancing and implementing the Brillouin optical frequency domain analysis, vol 64. BAM Dissertationsreihe
8. Schuller H, Schwingshackl I, Moser F, Lienhart W (2014) Semmering Basistunnel neu—geotechnisches Monitoring mit faseroptischen Messsystemen beim Bau von Bewehrte-Erde-Stützkonstruktionen in der Deponie Longsgraben. 29. Christian Veder Kolloquium: Stützmassnahmen in der Geotechnik—Bemessung, Ausführung, Langzeitverhalten 51:107–122
9. Schuller H, Schwingshackl I, Schachinger T, Moser F, Lienhart W (2014) Semmering Basistunnel neu - faseroptische Messsysteme zur Erfassung der Dehnungen beim Bau von Bewehrte-Erde-Stützkonstruktionen in der Deponie Longsgraben. Messen in der Geotechnik 2014(98):291–311